Particulate Science and Technology, 32: 404–411

ISSN: 0272-6351 print/1548-0046 online
DOI: 10.1080/02726351.2014.883657

Taylor & Francis
Taylor & Francis Group

Particle Tracking in Large Eddy Simulated Turbulent Channel Flow Using Generalized Lattice Boltzmann Method

MANDANA SAMARI KERMANI,[1] SAEED JAFARI,[2] MOHAMMAD RAHNAMA,[1] and MAZYAR SALMANZADEH[1]

[1]*Mechanical Engineering Department, Shahid Bahonar University of Kerman, Kerman, Iran*
[2]*Petroleum Engineering Department, Shahid Bahonar University of Kerman, Kerman, Iran*

The deposition of spherical solid particles with $0.00192 \leq \tau^{+} \leq 160.56$ in three-dimensional turbulent vertical and horizontal channel flows with friction Reynolds number $\mathrm{Re} = \frac{u_{\tau} * H}{\nu} = 180$ was studied. A generalized lattice Boltzmann equation (GLBE) was used for computation of instantaneous turbulent flow field for which large eddy simulation (LES) was employed. The subgrid scale (SGS) turbulence effects were simulated through a shear-improved Smagorinsky model (SISM), which can predict turbulent near wall region without any wall function. The Lagrangian particle tracking approach was used, and qualitative distribution of particles in a vertical channel center plane and in a near wall region was presented. It was shown that, in horizontal channels, the rate of deposition is higher than in vertical channels since gravitational sedimentation is the dominant mechanism of deposition on the lower wall. Combination of SISM in GLBE with particle tracking analysis in turbulent channel flow is the novelty of the present work. Since the accuracy of the flow field is essential to correctly predict particles' behavior, a reliable method should be used to simulate the flow field. In the proposed method, the flow field equations are solved locally. The collaboration of this method and particle tracking can be considered a good candidate for simulation of particulate flow.

Keywords: Large eddy simulation, generalized lattice Boltzmann equation, particle tracking, sedimentation, turbulent flow

Introduction

The importance of analyzing aerosols' behavior in turbulent flows lies in their wide range of applications. Improving microelectronic industries, filtration and separation processes, and cloud formation are a few examples that need understanding, measuring, and quantifying for the dispersion and deposition of microparticles suspended in turbulent flow fields. In order to provide a method for Lagrangian tracking of particles, interactions between turbulence eddies and particle motion must be considered. While very high inertia particles' movements may be insensitive to all but the mean flow structures, small inertia particles follow eddy streamlines even at smallest scales. So, instantaneous fluid velocity components have to be evaluated carefully. Direct numerical simulation (DNS) of flow field is the most accurate method, but its high computational expense makes it inapplicable for large Reynolds numbers (Re) or complex geometry applications. Reynolds averaged Navier-Stokes (RANS) models contain many empirical parameters that are determined from specific examples. Thus, the application of RANS is limited. Large eddy simulation (LES) is an approach intermediate to DNS and RANS. It has the ability to compute large scales directly, while modeling universal small scales with an appropriate subgrid scale (SGS) modeling. A number of studies that employed a Lagrangian model to track particles in wall-bounded turbulent flows have been reported. Experimental and theoretical studies related to particles behavior in turbulent flows were provided by Wood (1981) and Papavergos and Hedley (1984). Wang et al. (1997) proposed different expressions to calculate the optimum lift force on particles. Salmanzadeh et al. (2012) modeled the effect of thermal plume adjacent to the body on particle transport and showed that temperature gradient made an important role in transporting 1 μm particles. Zhang and Ahmadi (2000) studied particle deposition in vertical and horizontal duct flows using the DNS approach and showed that how particle-to-fluid density ratio, flow direction relative to gravity, and shear-induced lift force affect the flow field. Tian and Ahmadi (2007) simulated nano- and microparticle deposition in turbulent duct flows by two RANS models, that is, the $K-\varepsilon$ model and the Reynolds stress transport model (RSM). They also provided a comparative study of accuracy of various turbulence models for particles transport and deposition in duct flows. Using a subgrid scale (SGS) model, Wang and Squires (1996) used the LES method and generated SGS fluctuation velocities using random numbers sampled from a Gaussian distribution. Winkler et al. (2003) used SGS models to study preferential concentration of particles in a fully developed turbulent duct flow. In their study, it was seen that particles

Address correspondence to: Saeed Jafari, Petroleum Engineering Department, Shahid Bahonar University of Kerman, Kerman, Iran. E-mail: saeed.jafari.1362@gmail.com
Color versions of one or more of the figures in the article can be found online at www.tandfonline.com/upst.

accumulate in low vorticity regions. Salmanzadeh et al. (2010) developed a SGS model to study the effect of SGS turbulence fluctuations on particle dispersion and deposition processes. They showed SGS fluctuations increase the deposition rate. Jung et al. (2013) simulated turbulent duct flow using lattice Boltzmann method, and then allowed inertial particles to be tracked through a static probability density field distribution. Their results suggested that accurate particle tracking is feasible given a suitable probability field.

In the present study, application of shear-improved Smagorinsky model (SISM) in large eddy simulation of turbulent flow is used through a generalized lattice Boltzmann method (GLBM). In fact, lattice Boltzmann method (LBM) was used because of its important features that distinguish it from other numerical methods. First, the convention operator of the LBM in velocity space is linear. Second, the pressure in LBM is calculated using an equation of state. Third, the LBM utilizes minimal set of velocities in phase space. Since both GLBM and SISM do local calculations to solve the fluid velocity field, the method is easy coding and cost effective.

After solving the flow field, particles are tracked as they move under the influence of drag, lift, Brownian, and gravitational forces. The results were compared with available experimental data and empirical equations. It is worth mentioning that, to the best of authors knowledge, investigation of particles behavior with application of SISM in multi-relaxation time LBM for simulation of turbulent channel flow has not been studied before.

Simulation Procedure

Fluid Flow Simulation

LBM simulates fluid flow using fictitious particles groups in the form of a distribution function, which perform consecutive propagation and collision processes over a discrete lattice mesh. During collision step, distribution functions relax toward their local equilibrium values and in streaming process they move along the characteristic directions presented by the LBM model, Succi (2001). The effect of external forces such as pressure gradient can also be considered in an additional force term. GLBM computes the collision in moment space and streaming in velocity space. Since this method uses multiple relaxation times (MRT), it is more stable than single relaxation time (SRT) LBM. GLBE with forcing term can be written in the following form (Premnath 2009a):

$$f(\overrightarrow{X}+\overrightarrow{e}\delta t, t+\delta t) = f(\overrightarrow{X}, t) - M^{-1}\cdot\hat{s}\cdot [m - m^{eq}(\rho, \overrightarrow{U})](\vec{X}, t) + M^{-1}\cdot(I-\frac{1}{2}\hat{s}).S(\overrightarrow{X}, t) \quad (1)$$

In the present study, D3Q19 model was used to simulate the flow field so all the vectors in Equation (1) have 19 components. The last term in Equation (1) shows the effect of source terms in moment space which are functions of $\vec{F}$ and $\overrightarrow{U}$. Components of $S(\vec{X}, t)$, $\hat{s}$, m and m^{eq} are mentioned in Premnath et al. (2009a, 2009b) and Pattison (2009).

In D3Q19 model, the macroscopic density and momentum on each lattice node are calculated from Equations (2) and (3).

$$\rho = \sum_{\alpha=0}^{18} f_\alpha \quad (2)$$

$$\rho\overrightarrow{u} = \sum_{\alpha=1}^{18} \overrightarrow{e_\alpha} f_\alpha + \frac{1}{2}\overrightarrow{F}\delta_t. \quad (3)$$

In matrix $\hat{s}$, the relaxation rates that correspond to hydrodynamic modes can be related to transport coefficients and modulated by eddy viscosity due to SGS model as: $s_1^{-1} = 0.5(9\xi + 1)$, and $s_9 = s_{11} = s_{13} = s_{14} = s_{19} = s_\nu$ with

$$s_\nu^{-1} = 3\nu' + 0.5 = 3(\nu + \nu_T) + 0.5. \quad (4)$$

Other relaxation rates are indicated as: $s_1 = 1.19$, $s_2 = s_{10} = s_{12} = 1.4$, $s_4 = s_6 = s_8 = 1.2$, $s_{16} = s_{17} = s_{18} = 1.98$. (Humières et al. 2002; Yu et al. 2006; Premnath et al. 2009a).

Strain rate tensor components, used to model SGS turbulence, can be written in terms of non-equilibrium moments -h^{neq}. For instance:

$$S_{xx} \approx -\frac{1}{38\rho}\left[s_1 h_1^{neq} + 19 s_9 h_9^{neq}\right], \quad (5)$$

where

$$h_\alpha^{neq} = m_\alpha - m_\alpha^{eq} + \frac{1}{2}S_\alpha. \quad (6)$$

Other components can be found in Premnath et al. (2009b).

The magnitude of strain rate tensor,$|S|$, using strain rate tensor components can be calculated from Equation (7).

$$|S| = \sqrt{2S_{ij}S_{ij}} = \sqrt{2\left[S_{xx}^2 + S_{yy}^2 + S_{zz}^2 + 2(S_{xy}^2 + S_{yz}^2 + S_{xz}^2)\right]}. \quad (7)$$

Calculation of Eddy Viscosity with Shear-Improved Smagorinsky Model

In order to model turbulence in lattice Boltzmann method, a varying relaxation toward equilibrium (i.e., $\hat{s}$ in Equation (1)) was used. For computing subgrid scale stresses used in LES computations, shear-improved Smagorinsky model was implemented (Leveque et al. 2007). For SGS eddy viscosity evaluation, the magnitude of the shear should be subtracted from the instantaneous resolved rate of strain:

$$\nu_T^{SISM}(x,t) = (C_S\Delta)^2(|S_\Delta(x,t)| - S(x,t)) \quad (8)$$

$C_S = 0.18$ for homogeneous and isotropic turbulence and $\Delta = (\Delta x\Delta y\Delta z)^{\frac{1}{3}}$. Since the flow is assumed to be well enough resolved in the direction of the shear, then $S(x, t) \approx |\langle S_\Delta(x, t)\rangle|$ (Jafari and Rahnama 2011).

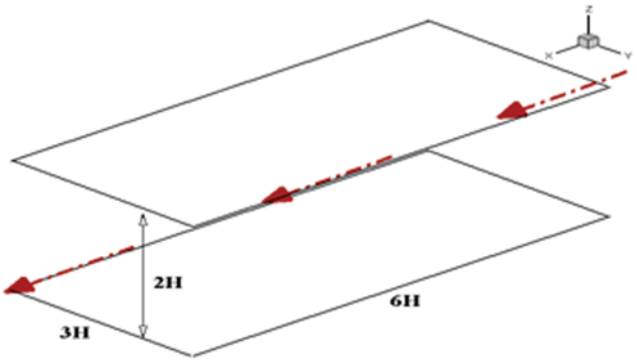

Fig. 1. Channel geometry.

In the present study, spatial averaging over homogeneous directions in the channel (i.e., x and y directions) was used to compute $|\langle S_\Delta(x,\ t)\rangle|$ and Equation (7) was employed for calculation of rate of strain. So ν_T^{SISM} was obtained from Equation (9) and was used as eddy viscosity in this turbulent flow.

$$\nu_T^{SISM}(x,t) = (C_S\Delta)^2(|S| - |\langle S_\Delta(x,t)\rangle|). \tag{9}$$

The total viscosity which is sum of the physical and the eddy viscosities is substituted in Equation (4).

Computational Domain

A schematic of fully developed channel flow having dimensions of $6H \times 3H \times 2H$ is presented in Figure 1. Reynolds number is 180, which previous DNS data are available for this Reynolds number.

The flow is bounded from top and bottom by two no-slip walls. Owing to presence of fully developed flow in stream-wise direction and homogeneity in span-wise direction, periodic boundary condition was selected for these two directions (Succi 2001).

The computational domain was discretized into $240 \times 120 \times 80$ nodes in stream-wise, span-wise and cross section directions, respectively. This corresponds to a mesh with resolution of 4.5 wall units in each direction. Because of using half-way bounce-back scheme for implementation of wall boundary condition, the first grid point is located at a distance of 2.25 wall units from the wall.

The driving force in the present channel flow is pressure gradient in flow direction and can be related to τ_w and u_τ through:

$$\vec{F} = -\frac{dp}{dx}\vec{i} = \frac{\tau_w}{H}\vec{i} = \frac{\rho u_\tau^2}{H}\vec{i}. \tag{10}$$

Particles Equation of Motion

Here, the dispersed phase is solved using a Lagrangian approach whereas the carrier phase is treated via an Eulerian approach as explained in previous sections. The effect of particles feedback force on the flow is negligible. The governing equations of motion are given by:

$$\frac{du_i^p}{dt} = \frac{1}{\tau}\frac{C_D\mathrm{Re}_p}{24}(u_i - u_i^p) + \frac{f_{lift}}{m_p} + (1 - \frac{1}{s})g_i + n_i(t) \tag{11}$$

$$\frac{dx_i}{dt} = u_i^p, \tag{12}$$

where

$$\tau = \frac{sd^2C_C}{18\nu}. \tag{13}$$

$$C_C = 1 + \frac{2\lambda}{d}(1.257 + 0.4e^{\frac{-1.1d}{2\lambda}}). \tag{14}$$

$$C_D = \begin{cases} \frac{24}{\mathrm{Re}_p} & \mathrm{Re}_p \prec 1 \\ \frac{24}{\mathrm{Re}_p}(1 + 0.15\mathrm{Re}_p^{0.687}) & 1 \prec \mathrm{Re}_p \prec 400 \end{cases} \tag{15}$$

and Re_p is based on the flow-particle slip velocity as:

$$\mathrm{Re}_p = \frac{d|u_{rel}|}{\nu}. \tag{16}$$

On the right-hand side of Equation (11), the first term considers the Stokes drag force. The second term represents the lift force and the third term accounts the buoyancy effect.

The lift force used in this study was the "optimum" one as defined by Wang et al. (1997). Different expressions for this force are specified by Saffman and Stokes length scales and dimensionless parameters ε and l^+.

$$L_G = \sqrt{\frac{\nu}{|G|}}.,\quad L_s = \frac{\nu}{|u_{rel}|}., \tag{17}$$

$$\varepsilon = sign(G|u_{rel}|)\frac{\mathrm{Re}_G^{1/2}}{\mathrm{Re}_p},\ l^+ = \frac{l}{L_G} \tag{18}$$

$$\mathrm{Re}_G = \sqrt{\frac{|G|d^2}{\nu}}. \tag{19}$$

If the distance of particle from the wall is lower than both L_s and L_G, the lift force is calculated by Equation (20) (Cherukat and McLaughlin 1994).

$$\begin{aligned} f_{lift} = \rho(\frac{d}{2})^2 * \left|u_i - u_i^p\right|^2 [&1.7716 + 0.2160 * k - 0.7292k^2 \\ &+ 0.4854k^3 - (3.239k^{-1} + 1.1450 + 2.0840k - 0.9059k^2)\Lambda \\ &+ (2.0069 + 1.0575k - 2.4007k^2 + 1.3174k^3)\Lambda^2] \end{aligned} \tag{20}$$

where

$$k = \frac{d}{2l},\ \Lambda = \frac{dG}{2u_{rel}}. \tag{21}$$

If the particle moves outside this region, the lift force takes the following form:

$$f_{lift} = -\frac{9}{\pi}\rho(\frac{d}{2})^2|u_i - u_i^p|\sqrt{\upsilon|G|}sign(G)J. \tag{22}$$

J contains two parts. One for considering the contribution of the velocity shear, J^u, and the other one for considering the wall effects, J^w. In this study, J^u and J^w are calculated using the procedure proposed by Wang et al. (1997). However, the difference is in the way of calculating I in the expression proposed by Vasseur and Cox (1997) which is:

$$J = -\frac{2\pi^2}{3|\varepsilon|} I + J^u. \tag{23}$$

The method used here is the same as the one used by Arcen et al. (2006) in which J is defined by different expressions according to various values of $l^+ = \frac{l}{L_s}$.

$$I = -3.1 * 10^{-4} * l^{*^4} + 3.53 * 10^{-3} * l^{*^3} - 1.088 * 10^{-2} * l^{*^2} - 9.86 * 10^{-3} * l^* + 9.57 * 10^{-2}. \tag{24}$$

$$I = 6.78 * 10^{-7} * l^{*^4} - 4.81 * 10^{-5} * l^{*^3} + 1.26 * 10^{-3} * l^{*^2} - 1.485 * 10^{-2} * l^* + 7.05 * 10^{-2}.\ \ 4.5 \prec l^* \leq 25 \tag{25}$$

$$\begin{aligned} I &= 0. \\ l^* &\geq 25. \end{aligned} \tag{26}$$

The last term is the Brownian force per unit mass that shows the impact of fluid molecules on particles and is modeled as a Gaussian white noise random process, and is evaluated at every time step, Δt, as:

$$n_i(t) = R_i \sqrt{\frac{\pi S_0}{\Delta t}}, \tag{27}$$

where R_i represents a zero-mean, unit variance independent Gaussian random number. The spectral intensity, S_0, is given as (Li and Ahmadi 1992):

$$S_0 = \frac{216 \nu K_b T}{\pi^2 \rho d^5 S^2 C_C}. \tag{28}$$

The interaction of particles with local turbulence is accounted for via using instantaneous fluid velocity field in Equation (11). In order to solve this equation, fluid velocity in particle location is needed and must be evaluated by an interpolation technique. Here, a volume averaged interpolation scheme was used (Salmanzadeh et al. 2010).

Deposition Velocity

In computer simulation, u_d and its dimensionless form, u_d^+, can be estimated as (Li and Ahmadi 1993a):

$$u_d = \frac{N_d / t_d}{N_0 / z_0}. \tag{29}$$

$$u_d^+ = \frac{u_d}{u_\tau}. \tag{30}$$

N_0 is the number of particles uniformly distributed within a distance z_0 from the wall and N_d is the number of deposited particles in the time interval t_d.

The results were reported in the form of u_d^+ versus τ^+ in order to compare them with available empirical models and experimental data, where

$$\tau^+ = \frac{\tau * u_\tau^2}{\nu}. \tag{31}$$

Wood (1981) suggested an empirical equation for non-dimensional deposition velocity as:

$$u_d^+ = 0.057 Sc^{-2/3} + 4.5 \times 10^{-4} \tau^{+^2} + \tau^+ g^+., \tag{32}$$

where $Sc = \nu / D$ is the Schmidt number with D being the particle mass diffusivity given as:

$$D = \frac{KT}{3\pi\mu d} C_C. \tag{33}$$

$$g^+ = \frac{\nu g}{u_\tau^3}. \tag{34}$$

Fan and Ahmadi (1993) developed an empirical equation for u_d^+ in which the effect of surface roughness and gravity along the flow direction is considered. This equation is defined as:

$$u_d^+ = \begin{cases} \{(0.084 Sc^{-2/3} \frac{1}{2} \left[\frac{(0.64k^+ + \frac{1}{2}d^+)^2 + \frac{\tau^{+^2} g^+ L_1^+}{0.01085(1+\tau^{+^2} L_1^+)}}{3.42 + (\tau^{+^2} g^+ L_1^+)/0.01085(1+\tau^{+^2} L_1^+)} \right]^{1/(1+\tau^{2^+} L_1^+)} & \text{if } u_d^+ \leq 0.14 \\ \quad \times \left[1 + 8e^{-(\tau^+ - 10)^2/32}\right] \frac{0.037}{1 - \tau^{+^2} L_1^+ (1 + (g^+ / 0.037))}). & \\ 0.14 & \text{Otherwise.} \end{cases} \tag{35}$$

Here, $L_1^+ = \frac{3.08}{sd^+}$, and k^+ is the surface roughness (that is set to zero for smooth surface in this study). For a horizontal channel, in which gravity is perpendicular to flow direction, $g^+ = 0$ in Equation (35) and the gravitational sedimentation velocity $\tau^+ g^+$ must be added.

Results and Discussion

Flow Simulation Results

In order to make sure about the accuracy of fluid velocity field, root-mean-square (RMS) fluctuation velocities were compared with RMS velocities obtained from DNS of Kim et al. (1987), and data from simulation of GLBE with Smagorinsky model of Premnath et al. (2009a). The results are in good agreement and are shown in Figure 2.

Particle Simulation Results

After reaching the flow field to a statistically steady state, in order to calculate particles' deposition velocity in vertical and horizontal channels, ensembles of 50,000 particles were randomly and uniformly distributed in half of the channel. The initial velocity of each particle was set equal to the local fluid velocity at particle's location. Instead of each deposited particle, another one was added in the channel half, randomly.

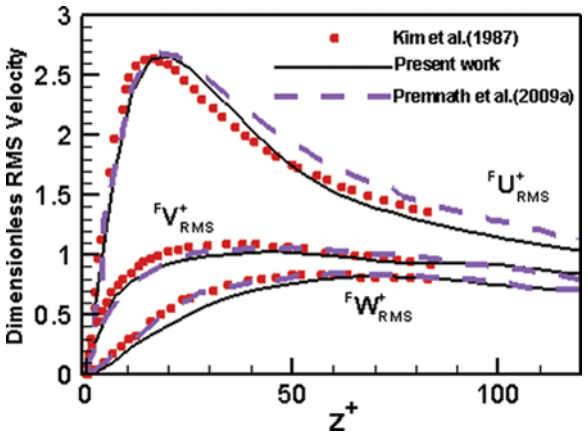

Fig. 2. Dimensionless RMS velocities versus distance from the wall.

To show particles concentration in vertical channels and how they distribute in center plane, 200,000 particles were distributed in whole channel and they were treated as before. All simulations were performed for $t^{+} = \frac{t^{*}u_{\tau}^{2}}{\nu} = 600$ and air flow at 288 K, $\nu = 1.5 \times 10^{-5} - \frac{m^2}{s}$, $u_{\tau} = 0.36\frac{m}{s}$, and $s = 2000$. The effect of re-bound was neglected.

Deposition Velocity in Vertical Channels

Figure 3 shows deposition velocity of particles versus their relaxation time in a channel with gravity in flow direction. The deposition velocity follows a "v-shaped" curve and then reaches the "saturation region" with constant u_d^{+}. The left side of the curve is called the "the Brownian region" in which molecular diffusion dominates deposition process. As the particle size decreases, the Brownian effect and the deposition rate increases. The right side is the "inertial region" where the deposition velocity is due to turbulent eddy impaction. u_d^{+} increases as the particle size increases. For τ^{+} greater than 10, due to particles' large inertia, the flow field does not have significant effect on their paths. Therefore, the deposition velocity approaches a constant value. Between Brownian and inertial regions there is a transition, where both molecular and inertial effects are small. So the deposition rate becomes minimum. The experimental

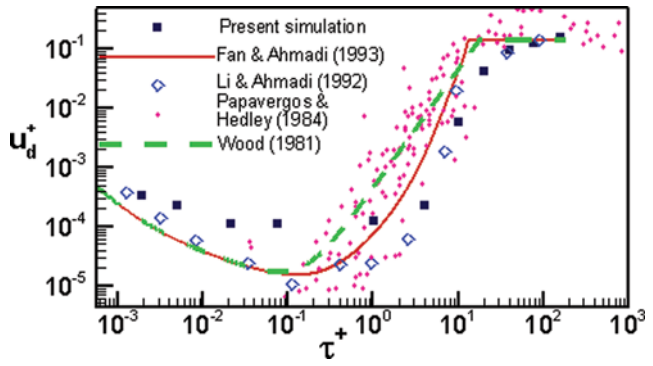

Fig. 3. Particle deposition velocity versus particle relaxation time in the presence of gravity in flow direction.

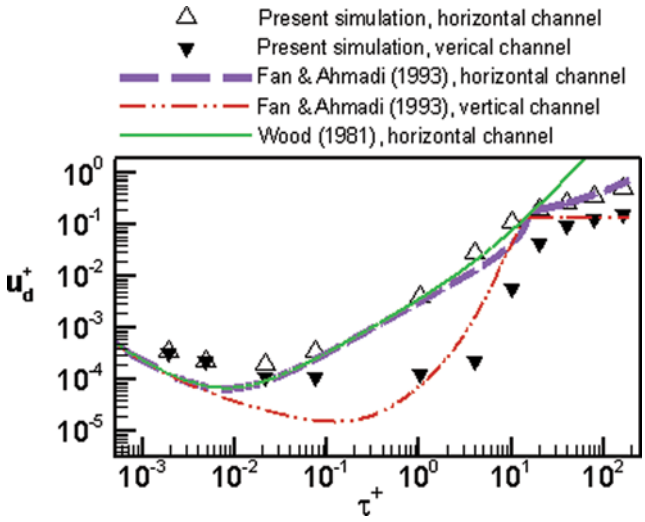

Fig. 4. Particle deposition velocity versus particle relaxation time in horizontal and vertical channels.

data of Papavergos and Hedley (1984), the empirical equation of Wood (1981), Fan and Ahmadi (1993), and the simulation results of Li and Ahmadi (1993b) are plotted in Figure 3 for comparison.

Deposition Velocity in Horizontal Channels

Figure 4 shows the simulated deposition velocity versus particles' relaxation time in channels with gravity perpendicular to flow direction. The predictions of Equations (32) and (35) are also presented for comparison. Similar to the case for the vertical channels, the deposition u_d^{+} follows a "v-shape" curve. But deposition is higher in the transition and the inertial regions due to the added deposition mechanism, which is gravitational sedimentation. In Brownian region, the gravity does not affect the deposition rate considerably since the molecular diffusion is the dominate mechanism for deposition.

Particles Distribution in a Vertical Channel

Figure 5 shows distribution of particles with different relaxation times in a vertical channel center plane, where the flow turbulence is homogeneous to some extent, at $t^{+} = 500.0$. As it was expected, flow follower particles ($\tau^{+} = 0.0216$) show random distribution because of the Brownian force effect on them. As particles become larger ($\tau^{+} = 4.0$, $\tau^{+} = 10.0$), they prefer to accumulate in definite streaks and they show a streaky distribution structure. However, this structure begins to diminish as τ^{+} increases beyond 20.0. Since, inertial particles do not obey all the flow structures and they remain unaffected. To get more precise and clearer picture of the particles distribution, location of particles has been shown along with the vorticity field in Figure 6. It is shown that definite structure of Figure 5d is because of the fact that particles with $\tau^{+} = 10.0$ are flung out of high vorticity regions into low vorticity regions.

In Figure 7, the accumulation of particles within the near wall region ($z^{+} = 6.75$), where the flow turbulence is not

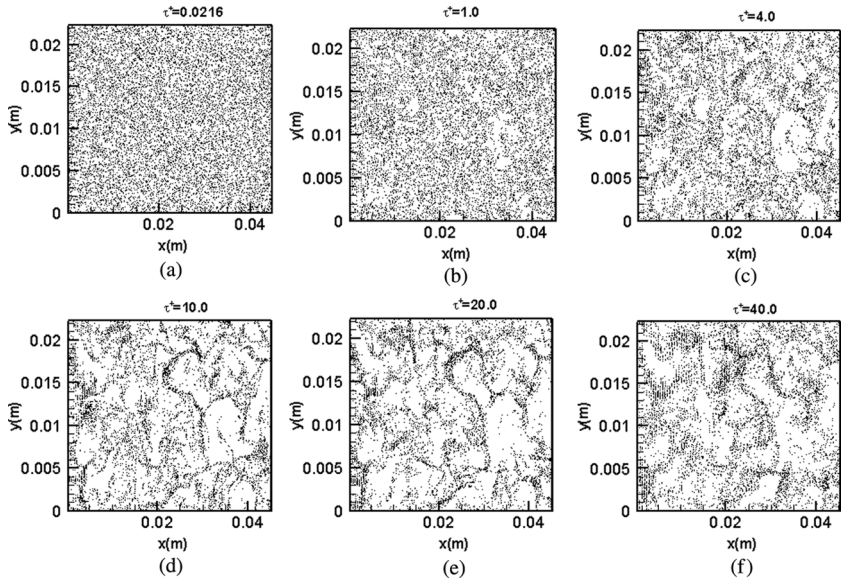

Fig. 5. Particle distribution at channel center plane for different relaxation times.

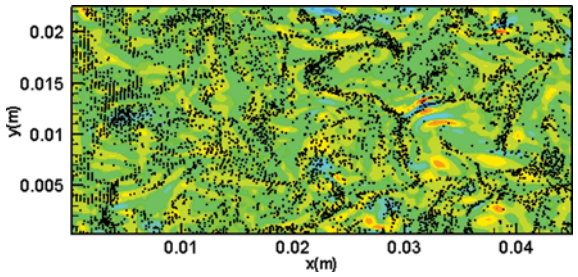

Fig. 6. Particle distribution and vorticity contours at channel center-plane ($\tau^+ = 10.0$).

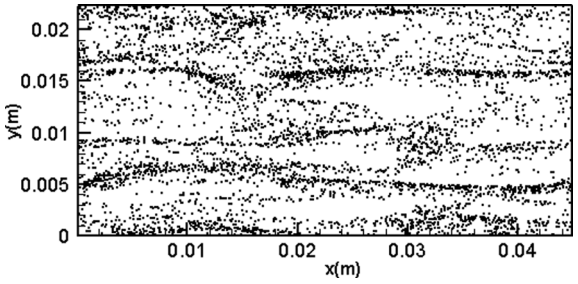

Fig. 7. Particle distribution at $4.75 \prec y^+ \prec 8.75$. ($\tau^+ = 10.0$).

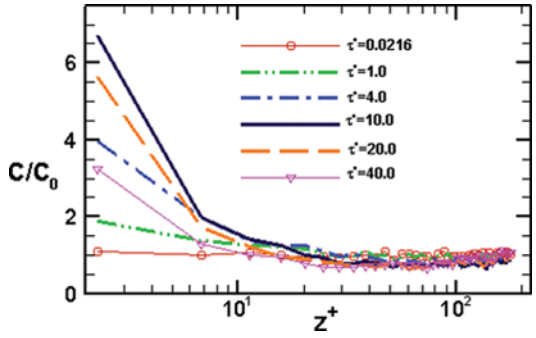

Fig. 8. Particle concentration versus the distance from the wall in vertical channels.

homogeneous, at $t^+ = 500.0$ is illustrated. It is seen that inhomogeneous turbulence has caused a different streaky distribution of particles in comparison with center plane distribution. These observations are in agreement with previous work of Wang and Squares (1996).

Particles Concentration in a Vertical Channel

Figure 8 displays the ratio of particles concentration, **C**, (number of particles in a definite volume), at $t^+ = 500.0$ to their initial concentration, $\mathbf{C_0}$, at $t^+ = 0.0$ versus dimensionless distance from the wall, where

$$z^+ = \frac{zu_\tau}{\nu}. \tag{36}$$

Although the Brownian particles ($\tau^+ = 0.0216$) concentration does not show a noticeable change in whole channel, profile of particles with $\tau^+ = 1.0$ depicts a slight increase near the wall. As τ^+ increases to 4.0 and 10.0, more particles accumulate in near wall region. Since, these particles are come near the wall through turbulent eddies but they cannot come upward again for they are larger than being guided only by flow. So, they are flung out of the eddies and their concentration grows where $z^+ \leq 10.0$. Despite such an upward trend, a reduction is seen in concentration of particles with $\tau^+ = 20.0$ and $\tau^+ = 40.0$. This is because of the fact that turbulent eddies cannot affect these inertial particles and they are large enough to deposit on the wall. So their concentration decreases.

Conclusions

In this study, the effect of gravity on particles' deposition rate in turbulent channel flows was studied. Also distribution of particles in vertical channel center plane and concentration

of them in near wall region were presented. The LES of turbulent flow was employed using a generalized lattice Boltzmann equation. SGS turbulent effects were simulated by SISM. One-way coupled Lagrangian particle tracking approach was used. The numerical simulation results for various cases were compared with previous available data. Following conclusions could be derived from the results.

- Both GLBM and SISM solve the fluid velocity field locally. The combination of the new method and particle tracking can be considered as a good candidate for simulation of particulate flow.
- In vertical channels on the left side of the v-shaped deposition velocity curve, Brownian effects become more significant as the particle relaxation time decreases. On the right hand side, by increasing particles' inertia the deposition velocity increases and approaches a constant value.
- When gravity is perpendicular to the flow direction, rate of particles deposition is higher than when it is in flow direction.
- Brownian particles show no preferential distribution, while larger particles prefer to locate in low vorticity regions.
- Particle distribution structure in center plane is different from its structure in near wall region.
- As τ^+ increases up to 10.0, more particles concentrate in near wall region. However, concentration decreases in this region, if τ^+ increases more.

Nomenclature

Cs	Smagorinsky constant
C_c	Stokes-Cunningham slip correction factor
C_D	drag coefficient
d	particle's diameter
dp/dx	pressure gradient
$\vec{e}_\alpha$	velocity vector in α direction
f	velocity distribution function
$\vec{F}$	external force vector of flow domain
g	gravity acceleration
g^+	Dimensionless gravity acceleration
G	wall-normal gradient of streamwise fluid velocity
H	channel half width
K_b	Boltzmann constant
l	distance of particle from the wall
L_G	Saffman's length scale
L_s	Stoke's length scale
m	moments vector
m^{eq}	equilibrium moments vector
m_p	particle's mass
M	transformation matrix of velocity space to moment space
Re	flow friction Reynolds number
Re_p	Particle Reynolds number
s	particle to fluid density ratio
S(x, t)	Shear at position x and time t
$\lvert S_\Delta(x, t)\rvert$	Magnitude of instantaneous resolved rate of strain
$S(\vec{X}, t)$	Source term vector
$\hat{s}$	diagonal matrix of relaxation rates
T	fluid absolute temperature
t	time
t^+	non-dimensional time
$\vec{U}$	fluid velocity vector
u_d	deposition velocity
u_d^+	dimensionless deposition velocity
u_i	fluid velocity in i direction
u_i^p	particle velocity in i direction
u_{rel}	Fluid-particle slip velocity
u_τ	shear velocity
x_i	particle position in i direction
z^+	dimensionless distance from the lower wall

Greek Letters

α	characteristic directions presented by the LBM model
Δ	filter width
λ	molecular mean free path of the gas
ν	fluid kinematic viscosity
ν_T	eddy viscosity
τ	particle relaxation time
τ^+	dimensionless particle relaxation time
τ_w	wall shear stress

References

Arcen, B., A. Taniere, and B. Oesterle. 2006. On the influence of near-wall forces in particle–laden channel flows. *International Journal of Multiphase Flow* 32:1326–1339.

Cherukat, P., and J. B. McLaughlin. 1994. The inertial lift on a rigid sphere in a linear shear flow field near a flat wall. *Journal of Fluid Mechanics* 263:1–18.

Fan, F. G., and G. Ahmadi. 1993. A sublayer model for turbulent deposition of particles in vertical ducts with smooth and rough surfaces. *Journal of Aerosol Science* 24:45–64.

Humières, D., I. Ginzburg, M. Krafczyk, P. Lallemand, and L. S. Luo. 2002. Multiple-relaxation- time lattice Boltzmann models in three dimensions. *Philosophical Transactions of the Royal Society* 360: 437–452.

Jafari, S., and M. Rahnama. 2011. Shear-improved Smagorinsky modeling of turbulent channel flow using generalized lattice Boltzmann equation. *International Journal of Numerica Methods in Fluids* 67: 700–712.

Jung, S., D. J. Phares, and A. R. Srinivasa. 2013. A model for tracking inertial particles in a lattice Boltzmann turbulent flow simulation. *International Journal of Multiphase Flow* 49:1–7.

Kim, J., P. Moin, and R. Moser. 1987. Turbulence statistics in fully developed channel flow at low Reynolds number. *Journal of Fluid Mechanics* 177:133–166.

Leveque, E., F. Toschi, L. Shao, and J. P. Bertoglio. 2007. Shear-improved Smagorinsky model for large-eddy simulation of wall-bounded turbulent flows. *Journal of Fluid Mechanics* 570: 491–502.

Li, A., and G. Ahmadi. 1992. Dispersion and deposition of spherical particles from point sources in a turbulent channel flow. *Journal of Aerosol Science and Technology* 16:209–226.

Li, A., and G. Ahmadi. 1993a. Computer simulation of deposition of aerosols in a turbulent channel flow with rough wall. *Journal of Aerosol Science and Technology* 18:11–24.

Li, A., and G. Ahmadi. 1993b. Deposition of aerosols on surfaces in a turbulent channel flow. *International Journal of Engineering Science* 31:435–451.

Papavergos, P. G., and A. B. Hedley. 1984. Particle deposition behaviour from turbulence flows. *Chemical Engineering Research and Design* 62:275–295.

Pattison, M. J., K. N. Premnath, and S. Banerjee. 2009. Computation of turbulent flow and secondaey motions in a square duct using a forced generalized lattice Boltzmann equation. *Physical Review E* 79(2):026704-1–026704-13.

Premnath, K. N., M. J. Pattison, and S. Banerjee. 2009a. Generalized lattice Boltzmann equation with forcing term for computation of wall bounded turbulent flows. *Physical Review E* 79(2):026703-1–026703-19.

Premnath, K. N., M. J. Pattison, and S. Banerjee. 2009b. Dynamic subgrid scale modeling of turbulent flows using lattice Boltzmann method. *Physica A* 388:2640–2658.

Salmanzadeh, M., M. Rahnama, and G. Ahmadi. 2010. Effect of subgrid scales on large eddy simulation of particle deposition in a turbulent channel flow. *Journal of Aerosol Science and Technology* 44:796–806.

Salmanzadeh, M., Gh. Zahedi, G. Ahmadi, D. R. Marr, and M. Glauser. 2012. Computational modeling of effects of thermal plume adjacent to the body on the indoor airflow and particle transport. *Journal of Aerosol Science* 53:29–39.

Succi, S. 2001. *The lattice Boltzmann equation for fluid dynamics and beyond*. Oxford University Press: Oxford.

Tian, L., and G. Ahmadi. 2007. Particle deposition in turbulent duct flows-comparison of different model predictions. *Journal of Aerosol Science* 38:377–397.

Vasseur, P., and R. G. Cox. 1977. The lateral migration of a spherical particles sedimenting in a stagnant bounded fluid. *Journal of Fluid Mechanics* 80:561–591.

Wang, Q., and K. D. Squires. 1996. Large eddy simulation of particle-laden turbulent channel flow. *Physics of Fluids* 8:1207–1223.

Wang, Q., K. D. Squires, M. Chen, and J. B. McLaughlin. 1997. On the role of the lift force in turbulence simulations of particle deposition. *International Journal of Multiphase Flow* 23:749–763.

Winkler, C. M., S. L. Rani, and S. P. Vanka. 2003. Preferential concentration of particle in a fully developed turbulent square duct flow. *International Journal of Multiphase Flow* 30:27–50.

Wood, N. B. 1981. A simple method for calculation of turbulent deposition to smooth and rough surfaces. *Journal of Aerosol Science* 12:275–290.

Yu, H., L. S. Luo, and S. Girimaji. 2006. LES of turbulent square jet flow using an MRT lattice Boltzmann model. *Journal of Computers and Fluids* 35:957–965.

Zhang, H., and G. Ahmadi. 2000. Aerosol particle transport and deposition in vertical and horizontal turbulent duct flows. *Journal of Fluid Mechanics* 406:55–80.